Flow instability prediction via eigenanalysis and its application to rotating stall

Shenren Xu [*1,2], Chen He [†3], Dakun Sun [‡3], and Dingxi Wang [§2]

[1]*Yangtze River Delta Research Institute of NPU, Northwestern Polytechnical University, Taicang 215400, P.R. China*
[2]*Northwestern Polytechnical University, Xi'an 710072, P.R. China*
[3]*Beihang University, Beijing 100191, P.R. China*

Global linear stability analysis is an effective way to predict the exact condition at which flow goes unstable. Compared to the time-domain simulation approach, eigenanalysis method can equivalently predict the destabilization condition, but at a much lower cost, since unsteady simulations are no longer required. In this work, a Newton–Krylov nonlinear flow solver is used to first solve for the steady state flow solution and then eigenanalysis is performed by applying the implicit-restart Arnoldi method to the exact Jacobian matrix. By tracking a subset of the eigenspectrum that is close to the imaginary axis, the least stable eigenmodes can be found. By perturbing the bifurcation parameter, e.g., the Reynolds number, the Hopf bifurcation point can be identified. This method is applied to find the critical Reynolds number for a laminar flow around a circular cylinder above which laminar vortex shedding appears. Time-accurate unsteady simulation confirms the correctness of the critical eigenvalue and eigenvector found. It is also applied to a quasi-3D compressor rotor annular cascade case, for which eigenanalysis is performed and flow physics is analyzed based on the unstable modes identified. Interesting correlation between the rotating perturbation pattern and cell rotating speed is found, which resembles what is observed in experiments. This work is a first step towards the study of rotating flow instabilities in turbomachines, such as rotating stall and rotating instability, and the preliminery results proved promising for future application to three-dimensional practical problems.

I. Introduction

Rotating stall and rotating instability have been studied extensively both experimentally [1–3] and numerically [4–7]. Early experimental work revealed the basic features of such phenemenon and subsequent work has focused on building simple analytical models. Existing analytical models [1, 8] have had their success in the early days but the accuracy and

[*]Associate Professor, School of Power and Engery; shenren_xu@nwpu.edu.cn
[†]Ph.D. Candidate, School of Energy and Power Engineering; hechen@ buaa.edu.cn (Corresponding Author)
[‡]Associate Professor, School of Energy and Power Engineering; Co-Innovation Center for Advanced Aero-Engine; sundk@buaa.edu.cn
[§]Professor, School of Power and Engery; dingxi_wang@nwpu.edu.cn

effectiveness of them is less than sastifactory when applied to realistic configurations and more details are needed for quantitative prediction of the stall behavior.

Previous numerical investigations mainly focused on using time-dependent unsteady flow analysis using either a fraction or the whole of an annulus. A lot of insight into the flow physics for the destablization mechanism has been gained from such high fidelity simuations. Unsteady simulations are useful for both reproducing the fully destabilized unsteady flows as well as for studying the inception of such instability. Due to the high computatioal cost of unsteady simulation, it still remains largely as a reserach tool to investigate the stall phenomenon on a case-by-case basis.

It is widely believed that the fully developed stall and surge behavior is quite different from the incipient stall, or pre-stall disturbance [9], as fully developed rotating stall exhibits strong nonlinearity. However, if the goal is to apply active control to suppress the instability at its infancy, then a linear stability prediction should suffice, as has been demonstrated in numerous work [10–13], as the idea is to eliminate the fully-developed rotating cells from forming.

As modern compression systems are designed with higher loading and speed, most analytical models proposed in the early days and desmontrated useful on low-speed machines are no longer useful as compressibility and complex flow mechanism such as boundary-layer-shock-wave interaction becomes important. In addition, existing models seldom take into account the exact geometry of the blading, and instead, a simple correlation of the compressor characteristics is used. This is obviously not desirable as geometry details, such as the exact leading edge geometry, have great impact on the stall characteristics. This is particularly the case when more complex stall phenomenon are considered, such as spike stall, where geometry details such as tip gap and the leading edge shape play a major role.

This calls for a stability analysis method based on the three-dimensional Reynolds-averaged Navier-Stokes equations, which is regarded as the standard industrial tool for predicting steady and unsteady turbomachinery performance. In a way, existing stall model needs to be upgraded using the latest high-fidelity flow models. Again, either time-dependent simulations or steady-state-based eigenanalysis can be used to study the stability based on the high-fidelity models and each has its strength. Time-dependent analysis is able to capture not only the incipent stall behavior but also the details of the transient process, but at a very high computational cost. Eigenvalue analysis is a powerful yet inexpensive tool to probe the flow near the critical condition, but is still capable of revealing rich flow physics, with cost comparable to a few steady state analysis.

In this work, we demonstrate that using eigenanalysis based on a whole-annulus steady state solution, the linear stablity demarcation point can be pinpointed with the cost of a few steady state analysis, and a full-annulus time-accurate unsteady calculation can thus be avoided. This methodology enables quick parametric study of the various rotating flow instability phenomenon such as rotating stall and rotating instability.

The idea of performing such eigenanalysis is simple. The difficulty is in the detail. One common misunderstanding is that an eigenanalysis for large cases is expensive. This is true only if we were to compute the full spectrum of a large sparse linear system using a direct method [14]. However, since a subset of the millions or even billions of eigenvalues

are relevant regarding the linear stability, typically $O(100)$, such eigenanalysis can be done at the cost of a few steady state analysis, using iterative eigenvalue calculation methods [15, 16].

In practice, such eigenanalysis is rarely done for large, complex cases of industry relevance. The challenge is twofold. First, in order to perform eigenanalysis, a steady state flow solution should first be obtained, requiring the full convergence of the flow solver. While this is easily achievable at design condition, obtaining a fully converged solution at off-design conditions remains a challange from the perspective of flow solver [17]. This is seldom discussed in literature, but widely felt in industry. Secondly, it is a common belief that the computatinal cost of such eigenanlysis is overwhelming and is thus impractical for real applications. With the maturing of distributed computing, this is no longer the bottleneck and one can easily compute the relevant eigenvectors for cases with up to 10 million grid point, and the cost only increases linearly with a scalable algorithm. But here the focus shifts slightly to the computational methods side from the flow physics . As discussed in [18], combining the advancement by computational specialists and the expertise from the 'stall fraternity' is the right way to advance the research in compressor stall study and an effective way to harness better the benifit of using CFD. In this paper, we attempt to apply the latest development in large scale eigenanalysis computational method to the long-standing problem of rotating flow instability, rotating stall in particular, and try to explore the underlying flow physics governing the pre- and in-stall behavior, at a computational cost that is affordable for industrial applications.

The rest of this paper is organized as follows. First, the basic algorithm of the nonlinear flow solver will be discussed in sec. II. Fundemantals of performing eigenanalysis based on RANS equations and relevant techniques are discussed in sec. III. Results for the application of eigenanalysis to predict flow instability is elaborated in sec. IV and conclusions are drawn in sec. V.

II. The nonlinear flow solver

The nonlinear flow solver used in this work is NutsCFD, an unstructured-mesh finite-volume RANS solver capable of dealing with rotating frame reference and periodic boundary conditions. The solver features the use of the Newton–Krylov algorithm, which significantly enhances the efficiency and robsutness when computing turbomachinery flows at off-design conditions. Details of the solver can be found in [19] and a brief description of the solution algorithm is provided in this section.

A. Governing equations

The integral form of the governing equations in a relative frame of reference with a constant angular velocity of ω is

$$\frac{d}{dt}\int_{\Omega_r}\mathbf{W}dV + \oint_{\partial\Omega_r}(\mathbf{F}_c^r - \mathbf{F}_v)dS + \int_{\Omega_r}\mathbf{F}_\omega dV = 0,$$

where $\mathbf{W}$ are the conservative variables $[\rho, \ \rho\mathbf{u}, \ \rho E]^T$. The absolute and relative convective fluxes, $\mathbf{F}_c$ and $\mathbf{F}_c^r$, the viscous flux $\mathbf{F}_v$, and the additional source term due to rotation, $\mathbf{F}_\omega$, are defined as

$$\mathbf{F}_c = \begin{bmatrix} \rho\mathbf{u}\cdot\mathbf{n} \\ \rho\mathbf{u}\mathbf{u}\cdot\mathbf{n} + p\mathbf{n} \\ \rho H\mathbf{u}\cdot\mathbf{n} \end{bmatrix}, \quad \mathbf{F}_c^r = \mathbf{F}_c - (\mathbf{u}_{rot}\cdot\mathbf{n}) \begin{bmatrix} \rho \\ \rho\mathbf{u} \\ \rho E \end{bmatrix}, \quad \mathbf{F}_v = \begin{bmatrix} 0 \\ \tau\cdot\mathbf{n} \\ \mathbf{u}\cdot\tau\cdot\mathbf{n} + \kappa\mathbf{n}\cdot\nabla T \end{bmatrix}, \quad \mathbf{F}_\omega = \begin{bmatrix} 0 \\ \rho\omega\times\mathbf{u} \\ 0 \end{bmatrix},$$

with $\mathbf{u}_{rot} = \omega \times \mathbf{x}$. When ω is zero, a solver applicable to non-rotating reference frame is recovered.

Flow is assumed to be fully turbulent and turbulence is modeled using the negative Spalart–Allmaras (SA-neg) model [20]. Compared to the original SA model [21], this avoids the clipping of the turbulent variable to a non-negative value which potentially prevents the full convergence of the nonlinear solver. The turbulence equation is discretized using the first-order accurate upwind scheme [22].

B. Spatial discretization

The governing equations are discretized using the method of lines and thus the spatial and temporal discretizations can be treated separately. The governing equations for the steady-state solution $\mathbf{W}$ is

$$\mathbf{R}(\mathbf{W}) = \mathbf{0}, \tag{1}$$

where $\mathbf{R}$ is the sum of fluxes and source terms associated with each control volume. Suppose control volume i has N flux faces with area S_{ik} for $k = 1, 2, ..., N$. R_i then is

$$R_i(\mathbf{W}) = \sum_{k=1}^{N} (\mathbf{F}_c^r - \mathbf{F}_v) S_{ik} + \mathbf{F}_\omega V_i,$$

where V_i denotes the volume. The computation of the convective flux $\mathbf{F}_c^r$ is based on a modification of the Roe flux scheme to account for the relative reference frame that is rotating with a constant angular velocity; while the viscous flux $\mathbf{F}_v$ is the same as in the stationary reference frame.

C. Temporal discretization

The Newton method solves the steady-state nonlinear equation (1) iteratively as

$$\mathbf{W}^{n+1} = \mathbf{W}^n + \beta\Delta\mathbf{W}$$

until convergence is reached, i.e., $\|\mathbf{R}(\mathbf{W})\| = 0$, where $\Delta\mathbf{W}$ is the solution to the linear system of equations

$$\frac{\partial\mathbf{R}}{\partial\mathbf{W}}\Delta\mathbf{W} = -\mathbf{R}(\mathbf{W}^n),$$

while β is an under-relaxation factor obtained using a line search.

Once the spatial discretization, $\mathbf{R}(\mathbf{W}^n)$, is established, there are three main steps to complete a Newton update step, namely, (i) forming the Jacobian matrix, (ii) solving the large sparse linear system of equations, and (iii) finding a step size β and update the nonlinear flow solution. To form the Jacobian matrix, automatic differentiatino tool Tapenade [23] is used, together with graph coloring tool Colpack [24]. By executing the foward-differentiated residual subroutine for a subsets of nodes with the same color, the Jacobian matrix is calculated. The resulting large sparse linear system of equations is solved using GMRES right-preconditioned by the incomplete LU factorization with zero fill-in.

III. Global linear stability analysis via eigenmode decomposition

A. Global linear stability analysis

A nonlinear dynamic system, e.g., the discretised NS equation discretized using the method of lines, has the form

$$Vol\frac{d\mathbf{u}}{dt} = -\mathbf{R}(\mathbf{u})$$

where $\mathbf{u}$ is the time-varying flow variable and $\mathbf{R}(\mathbf{u})$ is the nonlinear residual representing the spatial discretization. Vol is a diagonal matrix with the volume of each dual cell on its diagonal. This term can be eliminated by redefining $\mathbf{R}(\mathbf{u})$ by applying volume scaling to it. The governing equation of the dynamic system then becomes

$$\frac{d\mathbf{u}}{dt} = -\mathbf{R}(\mathbf{u})$$

Assuming a steady state solution $\mathbf{u}_0$ (equilibrium point of the dynamic system) exists, and the time-varying flow variable can be decomposed into the steady and the unsteady part

$$\mathbf{u} := \mathbf{u}_0 + \tilde{\mathbf{u}}$$

and the governing equation becomes

$$\frac{d\tilde{\mathbf{u}}}{dt} = A\tilde{\mathbf{u}}$$

where A is the negative Jacobian $A := -\dfrac{\partial\mathbf{R}}{\partial\mathbf{u}}$.

In order to use the eigen model decomposition approach, suppose the system matrix has right eigenvectors

$\{\mathbf{v}_i, \mathbf{v}_2, ..., \mathbf{v}_N\}$, which forms the matrix V as its colum vectors. Matrix A can then be factorized as

$$A = V\Lambda V^{-1}$$

where the diagonal matrix Λ has the eigenvalues of the matrix A as its diagonal elements. Decomposing the unsteady part $\tilde{\mathbf{u}}$ in the eigen modal space with coordinates η

$$\tilde{\mathbf{u}} = V\eta.$$

Substituting $\tilde{\mathbf{u}}$ in the governing equation using the eigen modal decomposition, it becomes

$$\frac{d\eta}{dt} = \Lambda\eta.$$

All equations are decoupled now and can be written as

$$\frac{d\eta_i}{dt} = \lambda_i\eta_i \quad \forall i.$$

For the linear system to be stable, a sufficient condition is that all eigenvalues have negative real parts, i.e., $\text{real}(\lambda_i) < 0, \forall i$.

B. Numerical implementation of eigenanalysis

In theory, performing the global linear stability analysis as described above is a standard procedure involving three steps: (i) find an equilirium point $\mathbf{u}_0$; (ii) linearize the nonlinear residual and form the Jacobian matrix A, and (iii) perform eigenanalysis and find Λ and V. Step (i) is simply running the steady state flow solver until a steady state solution is found. Step (ii) is a by-product of the nonlinear flow calculation using the NK method, i.e., store away the Jacobian matrix at the final Newton step. Step (iii) is a bit more involved for high dimensional problems.

For eigenmode computations, the implicitly restarted Arnoldi method proposed by Sorensen [15] and implemented in the ARPACK library [16], is used in combination with the NutsCFD solver. Shift-and-invert spectral transformation is applied to converge to wanted parts of the eigenspectrum, and critical is therefore the robust solution of many linear systems of equations. Key to efficiently solving the arising large sparse linear system of equations is the deflated Krylov subspace solver GCRO-DR [25]. Compared with the more commonly used GMRES solver [26], GCRO-DR is both more CPU time and memory efficient, especially as the system matrix condition worsens, as demonstrated in [27, 28].
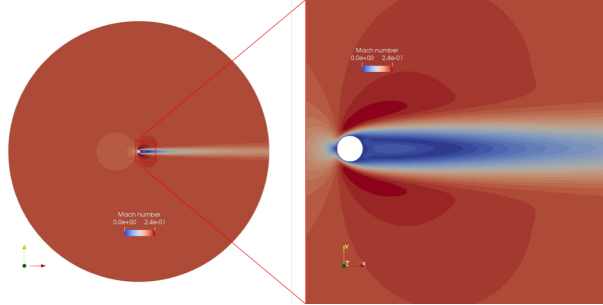
IV. Results

A. Laminar flow around a two-dimensional circular cylinder

Eigenvalue analysis is performed for the canonical case of the laminar flow around a circular cylinder with the Reynolds number in the range between 40 and 100. The computational domain is a circular cylinder centered at the origin with a diameter of $D = 10^{-5}$ and the farfield is a circle with a diameter of $100D$. The left half of the outer circle is set to 'farfield' boundary condition with an incoming flow of Mach 0.2 in the x-direction, a static pressure of 101325 Pa and and a temperature of 288.15 K. The right half of the circle is set to 'pressure-outlet' boundary condition, with a constant pressure of 101325 Pa. The computational domain is meshed with quadrilateral elements, with a total of 29600 grid points. The density is 1.225 kg/m^3. The dynamic viscosity is varied in order to achieve a particular Reynolds number.

1. Steady state calculation

The steady state flow solution for $Re = 55$ is obtained by either using an implicit solution method in Fluent (version 19.2) or by resorting to the Newton-Krylov algorithm in NutsCFD, despite the fact that the flow is physically unsteady under this condition. The Mach number contour of the NutsCFD calculation is shown in Fig. 1.


Fig. 1   Mach number contour plot of the calculation results by NutsCFD for $Re = 55$.

To compare the Fluent and NutsCFD results quantitatively, the x-velocity behind the cylinder and the pressure coefficient along the cylinder surface are presented in Fig. 2 and very good agreement can be found.

2. Unsteady calculation

Experimental results show that the laminar flow around the cylinder becomes unsteady for Re above a critical value (around 47). To study this phenomenon, unsteady flows for $Re = 55$ and $Re = 40$ are performed using NutsCFD. First, for both conditions, a steady state flow solution is obtained by converging the residual to machine error. Then, unsteady simulation is run with the steady state as the initial condition for $Re = 55$. A BDF2 second-order implicit dual-time-stepping method is used with the physical time step set to $10^{-8} sec$, that is, $0.01ms$, and the inner loop is solved with a maximum of 3 Newton iterations. From Fig. 3, it can be seen that after around $100ms$, the lift coefficient starts to
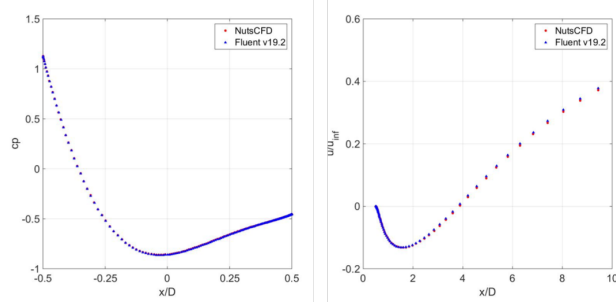
Fig. 2 Comparison between Fluent and NutsCFD calculation results for x-velocity along the center line behind the cylinder (left) and pressure coefficient along the cylinder surface (right).

grow and eventually reaches a saturated limit cycle at around $130ms$. On the contrary, running unsteady simulation with a fully converged steady state for $Re = 40$ does not lead to unsteadiness. To probe the flow at $Re = 40$ further, a disturbance is introduced into the flow from the farfield by setting the incoming flow direction to vertical for one time step and switching it back to the x-direction, and then continue the unsteady run. The lift coefficient shows a transient growth but eventually slowly delays to zero. The two sets of lift coefficient signals for $Re = 40$ and $Re = 55$ are plotted in Fig. 3 in both linear and logrithm scales. The logrithmic plot on the right clearly shows an exponential growth/decay for $Re = 55$ and $Re = 40$, respectively.
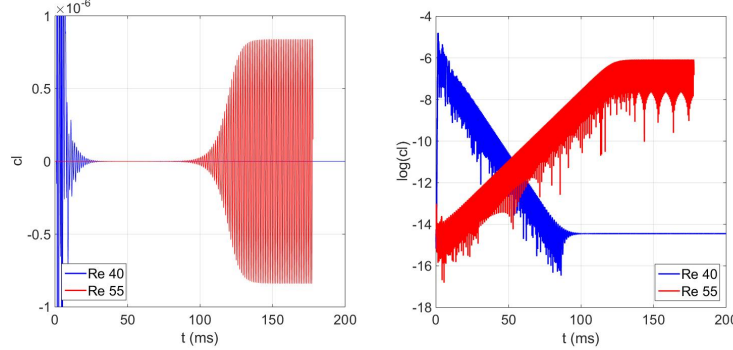

Fig. 3 Lift coeffient histogram for $Re = 55$ and $Re = 40$.

3. Eigenanalysis

Eigenanalysis is performed for the steady state solution calculated using NutsCFD. After converging the steady state solver to machine error ($tol = 10^{-14}$), the exact Jacobian matrix based on the 2nd-order spatial accuracy is calculated and output to file. ARPACK is used to computed a subset of the eigenvalues, with the aim of finding the least stable mode. To minimize the computational effort, 10 eigenvalues/vectors are computed for matrices with different shifts of 0, i, $2i$, $3i$, $4i$, $5i$. All the eigenvalues, 60 in total and with some duplicated, are plotted in Fig. 4. It can be seen that there is one eigenvalue that is on the right side of the imaginary axis, indicating there is one unstable mode. In the meantime,

8

from the time-domain simulation, one can extract from the lift-coefficient signal that the flow is exponentially growing with a growth rate of 0.123 and oscillating with a circular frequency of 4.94 rad/s. This value is plotted along with the spectrum and it can be seen that it overlaps with the unstable eigenvalue from the eigenanalysis.
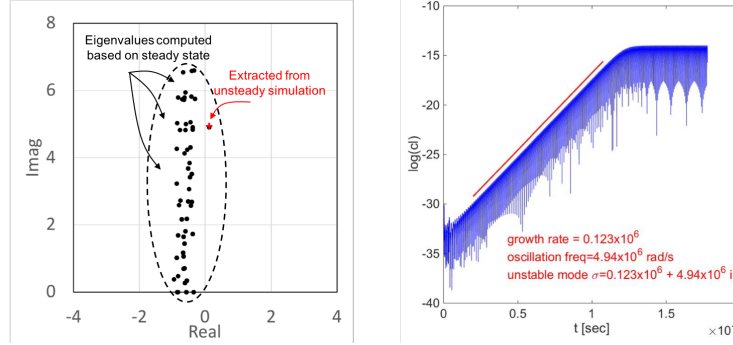
Fig. 4   Eigenspectrum from the steady state eigenvalue analysis compared with the linearly destabiling unsteady simulation for $Re = 55$**.**

The eigenanalysis not only generates the eigenvalues but also the eigenvectors associated with each eigenvalue. For the unstable mode, the real part of the density, x/y momentum and energy component of the unstable eigenvector is shown in Fig.5. Although not further explored here, these eigenvectors will be useful for constructing reduced-order-models, which can be used for rapid parametric study or fast time-domain responce.
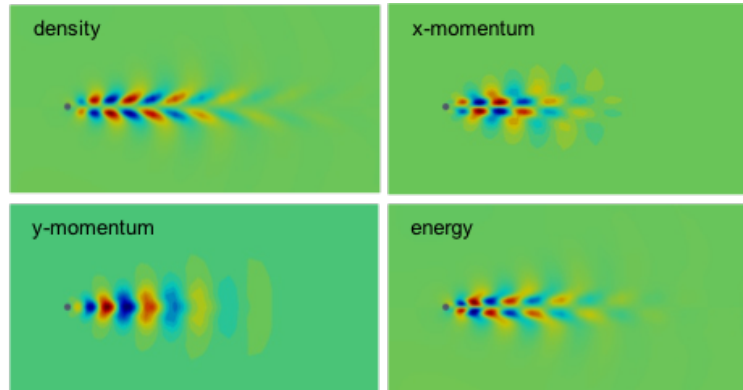
Fig. 5   Real part of the density, x/y momentum, energy components of the unstable eigenmode for $Re = 55$**.**

4. Bifurcation tracking

The same procedure for computing the eigenvalues for $Re = 55$ is applied to flows at $Re = 40$, 45, and 50 to obtain their respective spectra, which is shown in Fig. 6. It can be seen that as the bifurcation parameter Re is increased from 40 to 55, one eigenmode becomes linear unstable. The real part of this eigenvalue is plotted against Re on the right in Fig. 6. It across the imaginary axis at approximately $Re = 49$, consistent with the experimental value of $Re_{crit} = 47$. Note that shown in the figure is only the upper half of the spectrum and the complex conjugate of the destabilizing

9
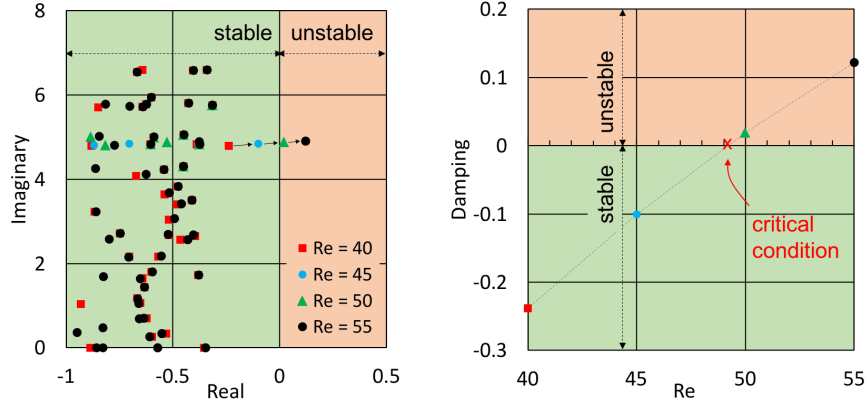
Fig. 6 The spectra for Re = 40, 45, 50 and 55 (left) and the damping v.s. the Reynolds number (right).

eigenvalue is thus not visualized. This is a classic Hopf bifurcation as the conjugate complex eigenpair destabilizes simultaneously. However, it should be noted that although linear stability analysis can predict the exact bifurcation, frequency predicted based on the unstable eigenvalue beyond that critical bifurcation parameter, Re_{crit}, should be used with care as it is different from the vortex shedding frequency except very close to onset, for the laminar flow around a long cylinder [29]. The implication on general cases is yet to be explored in future work.

### B. Transonic flow for an isolated rotor row (quasi-3D analysis)

NutsCFD is used to analyze the performance of the first stage rotor (NASA Rotor 67) of a two stage transonic fan designed and tested at the NASA Glenn center [30]. Its design pressure ratio is 1.63, at a mass flow rate of 33.25 kg/sec. The NASA Rotor 67 has 22 blades with tip radii of 25.7 cm and 24.25 cm at the leading and trailing edge, respectively, and a constant tip clearance of 1.0 mm. The hub to tip radius ratio is 0.375 at the leading edge (TC = 0.6% span) and 0.478 at the trailing edge (TC = 0.75% span). The design rotational speed is 16,043 RPM, and the tip leading edge speed is 429 m/s with a tip relative Mach number of 1.38.

As a first step, the analysis is performed on the surface of revolution taken at approximately 50% of the blade height. The three-dimensional mesh has one cell in the radial direction and the subsequent analysis is thus a quasi-3D one.
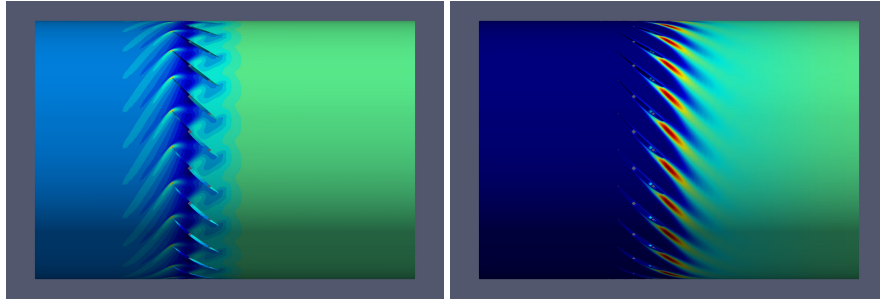
1. Steady state calculation

Steady state analysis is performed for both the single-passage and whole-annulus configurations. In order to obtain the steady state solutions for the whole annulus, which presumably is identical for each blade passage, we first compute the steady state solution for one passage with rotatioal periodicity, and then copy the solution to the whoe annulus using rotational transformation. Due to the slight difference in discretization, a fully-converged flow solution for one-passage produces a finite residual after it is copied to the whole annulus, and therefore a few extra iterations are required on the whole-annulus mesh to fully converge the flow to machine error. The pressure ratio and efficiency are shown in Fig. 7

which is produced by incrementally raising the back pressure from the inlet total condition. It can be seen that there is a small difference (mainly efficiency) between the single-passage and whole-annulus results, which is due to the minor discrepancy of the spatial discretization at the periodic boundaries for single passage calculation. The flow solution using the whole annulus is shown in Fig. 8. No mesh convergence study has been performed.
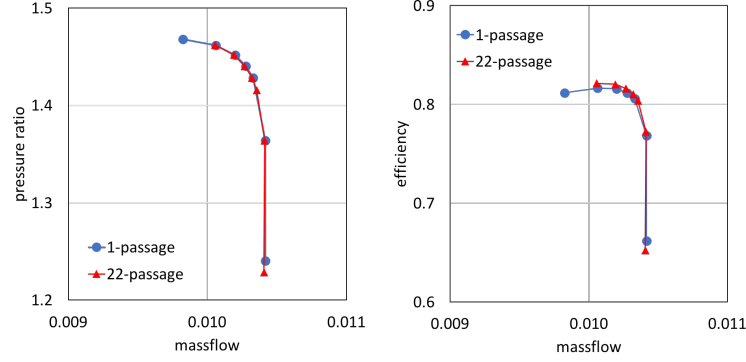
**Fig. 7   Q3D performance for rotor67 at 50% blade height with either single passage or whole annulus.**

Fig. 8   Pressure (left) and SA variable (right) contours for whole-annulus calculations.

2. Eigenanalysis

For each whole-annulus steady state solution, eigenanalysis is performed using the Jacobian matrix output from the NutsCFD solver once the steady state calculation has fully converged. Since the rotational speed for the rotor is 16043 RPM, the Jacobian matrix is scaled by a factor of $1/(2\pi \times 16043/60) \approx 1/1680$, so that all frequencies involved in this computation is normalized by the shaft angular frequency. This is done due to the pre-knowledge that rotating stall cells move with a speed of the same order of magnitude as the shaft speed.

Once the flow has fully converged, the left most point on the whole-annulus performance curve is used for eigenanalysis. Shown in Fig. 9 is a subset of the eigenvalues that are near the imaginary axis, which presumally are most likely to be unstable. ARPACK is used with various imaginery shifts to compute interior eigenvalues. The ones that are suspicious of crossing the imaginery axis are shown. A zoomed view of the eigenvalues reveals that there are a total of five that have positive real parts, i.e., unstable. A single-mode instability is not found for the case most likely

because the flow condition chosen is one that is deep into the linearly unstable region and a bifurcation point should be searched for at a higher flow-rate condition. Nevertheless, in the work, we restrict outselves to the analysis of this single condition and a thorough exploration of the whole picture will be conducted in our future work.
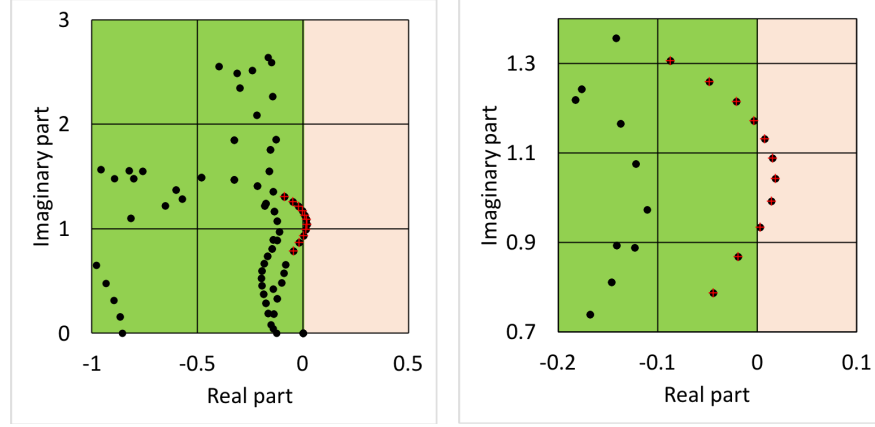
Fig. 9   Spectrum for stall condition.

The unstable eigenvector with the smallest imaginary part (lowest point among the five unstable eigenvalues) is visualized in Fig. 11 with both the real and imaginary parts. The circumferential shock oscillation can be seen. To analyze the spatial modes, data along the intersecting curve is taken (marked at the red line in Fig. 11). This is done for each of the 11 modes (marked with red cross in Fig. 9). It is clear from the spatial Fouriour analysis that each eigenvector corresponds to a rotating pattern with a different nodal diameter, which increases from 1 to 11 monotonically from the lowest to the highest eigenvalues.
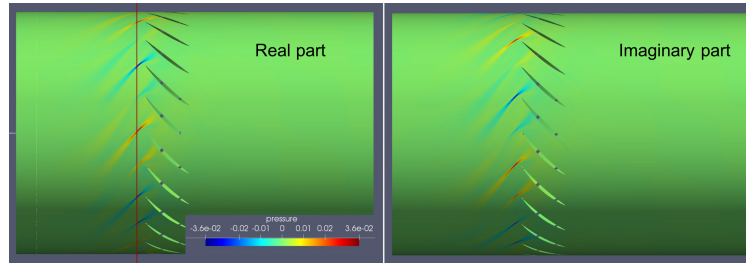

Fig. 10   Eigenvector 5 visualized using the real and imaginary parts of energy component

A more involved data processing reveals that the perturbation pattern, for every eigenvector, is a travelling wave that rotates in the opposite direction of the motion of the rotor (in the relative frame), and with a speed a fraction of the shaft rotating speed. This relative rotating speed can be calculated using the imaginary of the eigenvalue and the nodal diameter of the perturbation pattern as $\dfrac{\text{Imag}(\lambda)}{\omega_{shaft}} \dfrac{1}{ND}$. In the absolute reference frame, the cell rotating speed

(normalized with shaft angular frequency) is calculated as

$$U_{cellRotating} = 1 - \frac{\text{Imag}(\lambda)}{\omega_{shaft}} \frac{1}{ND}. \tag{2}$$

Applying this formula to each of the 11 eigenmodes leads to the correlation between the nodal diameter and the perturbation rotating speed, as shown in Fig. 11. Note that we use the terminology 'cell rotating speed' to be consistent with the language used by experimentalists when they describe the rotating cells. In fact, what is meant in the current context is actually 'rotating speed of the perturbation pattern'. Although it is well-known that the conclusions drawn from a global linear stability analysis can not represent the behavior of a saturated limit cycle which is highly nonlinear, it seems that the characteristics of the rotating perturbation, in terms of nodal diameter and rotating speed, is qualitatively representative of rotating cells observed experimentally. However, questions such as which eigenmode should destabilizes first, and how does the inlet distortion and blade-row interaction in multirow configuration affect the conclusion, remain to be answered.
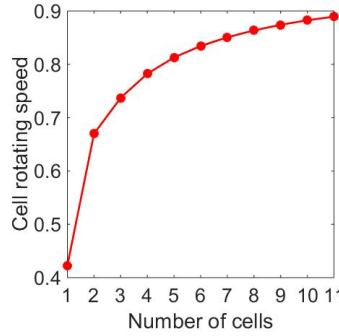
Fig. 11   The cell rotating speed in the absolute frame of reference v.s. the number of cells (nodal diameter of the perturbation pattern).

V. Conclusion

Rotating flow instability at near stall condition for an annular compressor cascade is studied using the eigenanalysis approach and the destabilizing eigenmodes are computed and analyzed to shed insight on the rotating stall phenomenon. This is the first time a full-order gloabl linear stability analysis based on the three dimensional RANS equations is performed to study the destabilising mechanism of such turbomachinery flow phenomenon.

Specifically, a stable nonlinear flow solver based on the matrix-forming Newton–Krylov approach is used to compute the steady state flow solution at near stall (possibly post-stall) condition and the readily available exact Jacobian matrix is then used for eigenvalue anlaysis. The eigenanalysis is performed to compute a subset of the eigenvalues that are near the imaginary axis, with the implicit-restarted Arnoldi method implemented in the ARPACK library. The shift-and-invert approach is used to obtain the least unstable eigenvalues.

The methodology is first applied to the classic case of a laminar flow around a 2D circular cylidner. By perturbing the system parameter *Re*, Hopf bifurcation is identified which is responsible for the inception of the laminar vortex shedding. The frequency and linear growth ratio from the eigenanalysis agree well with time-dependent simulation during the linear growth regime.

The same procedure is then applied to the a quasi-3d compressor rotor. Analysis shows the existance of a complete set of spatial modes that have different nodal diameters and rotating speeds. These analysis results provide a solid foundation for the explanation of various observations in experiments regarding rotating flow instabilities. It is revealed that the multiple modes with different nodal diameters coexist, as the inherent property of the physical system, and it can be hypothesized that the reason for different observed stall cell patterns is due to one particular mode being excited to finite amplitute first by external disturbance. Further more, by processing the spatial modes and the imaginary part of the eigenvalues, rotating speeds of the perturbation patterns can be calculated and are found to qualitatively agree with the various experimentally observed values for rotating stall cells.

The preliminary results presented in this paper represent our first attempt to use eigenanalysis based on RANS equations to study the rotating flow instability phenomenon in turbomachinary flows. The results are promising in that it shows the eigenanalysis method is feasible for practical cases and the eigenvectors do capture some of the key featuers of the flow instability investigated. However, more in-depth study is needed to investigate the bifurcation process for the quasi-3D case, and further investigation into three-dimensional cases will be carried out in our future work.

Acknowledgements

References

[1] Emmons, H., "Compressor surge and stall propagation," *Trans. of the ASME*, Vol. 77, No. 4, 1955, pp. 455–467.

[2] Marble, F. E., "Propagation of stall in a compressor blade row," *Journal of the Aeronautical Sciences*, Vol. 22, No. 8, 1955, pp. 541–554.

[3] Emmons, H., Kronauer, R., and Rockett, J., "A survey of stall propagation–experiment and theory," *Journal of Basic Engineering*, Vol. 81, No. 3, 1959, pp. 409–416.

[4] Cornelius, C., Biesinger, T., Galpin, P., and Braune, A., "Experimental and computational analysis of a multistage axial compressor including stall prediction by steady and transient CFD methods," *Journal of Turbomachinery*, Vol. 136, No. 6, 2014, p. 061013.

[5] He, L., "Computational study of rotating-stall inception in axial compressors," *Journal of Propulsion and Power*, Vol. 13, No. 1, 1997, pp. 31–38.

[6] Vo, H. D., Cameron, J. D., and Morris, S. C., "Control of short length-scale rotating stall inception on a high-speed axial compressor with plasma actuation," *ASME Turbo Expo 2008: Power for Land, Sea, and Air*, American Society of Mechanical Engineers, 2008, pp. 533–542.

[7] Pullan, G., Young, A., Day, I., Greitzer, E., and Spakovszky, Z., "Origins and structure of spike-type rotating stall," *Journal of Turbomachinery*, Vol. 137, No. 5, 2015, p. 051007.

[8] Greitzer, E., and Moore, F., "A theory of post-stall transients in axial compression systems: part II—application," *ASME J. Eng. Gas Turbines Power*, Vol. 108, No. 2, 1986, pp. 231–239.

[9] Stenning, A., "Rotating stall and surge," *Journal of Fluids Engineering*, Vol. 102, No. 1, 1980, pp. 14–20.

[10] Paduano, J., Epstein, A., Valavani, L., Longley, J., Greitzer, E., and Guenette, G., "Active control of rotating stall in a low speed axial compressor," *ASME 1991 International Gas Turbine and Aeroengine Congress and Exposition*, American Society of Mechanical Engineers, 1991, pp. V001T01A036–V001T01A036.

[11] DAY, I., "Active Suppression of Rotating Stall and Surge in Axial Compressors," *J. Turbomach.*, Vol. 115, 1993, pp. 40–47.

[12] Paduano, J. D., Greitzer, E., and Epstein, A., "Compression system stability and active control," *Annual review of fluid mechanics*, Vol. 33, No. 1, 2001, pp. 491–517.

[13] Day, I., Breuer, T., Escuret, J., Cherrett, M., and Wilson, A., "Stall inception and the prospects for active control in four high speed compressors," *ASME 1997 International Gas Turbine and Aeroengine Congress and Exhibition*, American Society of Mechanical Engineers, 1997, pp. V004T15A022–V004T15A022.

[14] Amestoy, P. R., Duff, I. S., L'Excellent, J.-Y., and Koster, J., "MUMPS: a general purpose distributed memory sparse solver," *International Workshop on Applied Parallel Computing*, Springer, 2000, pp. 121–130.

[15] Sorensen, D. C., "Implicit application of polynomial filters in a k-step Arnoldi method," *SIAM journal on matrix analysis and applications*, Vol. 13, No. 1, 1992, pp. 357–385.

[16] Lehoucq, R. B., Sorensen, D. C., and Yang, C., *ARPACK users' guide: solution of large-scale eigenvalue problems with implicitly restarted Arnoldi methods*, Vol. 6, SIAM, 1998.

[17] Xu, S., Radford, D., Meyer, M., and Müller, J.-D., "Stabilisation of discrete steady adjoint solvers," *Journal of Computational Physics*, Vol. 299, 2015, pp. 175–195.

[18] Day, I., "Stall, surge, and 75 years of research," *Journal of Turbomachinery*, Vol. 138, No. 1, 2016, p. 011001.

[19] Xu, S., Mohanamuraly, P., Wang, D., and Müller, J.-D., "A parallel Newton–Krylov RANS solver for turbomachinery aerodynamic analysis at off-design conditions," *submitted*, 2019.

[20] Allmaras, S. R., and Johnson, F. T., "Modifications and clarifications for the implementation of the Spalart–Allmaras turbulence model," *Seventh international conference on computational fluid dynamics (ICCFD7)*, 2012, pp. 1–11.

[21] Spalart, P. R., and Allmaras, S. R., "A one equation turbulence model for aerodinamic flows," AIAA-CP 92-439, 1992.

[22] Langer, S., "Agglomeration multigrid methods with implicit Runge–Kutta smoothers applied to aerodynamic simulations on unstructured grids," *Journal of Computational Physics*, Vol. 277, 2014, pp. 72–100.

[23] Hascoët, L., and Pascual, V., "The Tapenade Automatic Differentiation tool: Principles, Model, and Specification," *ACM Transactions On Mathematical Software*, Vol. 39, No. 3, 2013.

[24] Gebremedhin, A. H., Nguyen, D., Patwary, M. M. A., and Pothen, A., "ColPack: Software for graph coloring and related problems in scientific computing," *ACM Transactions on Mathematical Software (TOMS)*, Vol. 40, No. 1, 2013, p. 1.

[25] Parks, M., de Sturler, E., Mackey, G., Johnson, D., and Maiti, S., "Recycling Krylov subspaces for sequences of linear systems," *SIAM Journal on Scientific Computing*, Vol. 28, No. 5, 2006, pp. 1651–1674.

[26] Saad, Y., and Schultz, M., "GMRES: A generalized minimal residual algorithm for solving nonsymmetric linear systems," *SIAM Journal on scientific and statistical computing*, Vol. 7, No. 3, 1986, pp. 856–869.

[27] Xu, S., Timme, S., and Badcock, K., "Enabling off-design linearised aerodynamics analysis using Krylov subspace recycling technique," *Computers & Fluids*, Vol. 140, 2016, pp. 385–396.

[28] Xu, S., and Timme, S., "Robust and efficient adjoint solver for complex flow conditions," *Computers & Fluids*, Vol. 148, 2017, pp. 26–38.

[29] Barkley, D., "Linear analysis of the cylinder wake mean flow," *Europhysics Letters*, Vol. 75, No. 5, 2006, p. 750.

[30] Strazisar, A. J., Wood, J. R., Hathaway, M. D., and Suder, K. L., "Laser anemometer measurements in a transonic axial-flow fan rotor," 1989.